(一社)日本リモートセンシング学会九州支部平成 29 年度研究発表会論文集

平成 30 年 2 月 17 日(土)
長崎大学工学部 10 番講義室

Investigation of agricultural water demands and the future prediction in Balkh Province, Afghanistan

○Abdullah Jami[1], Masahiro Tasumi[1]

Abstract: This study investigates the present conditions of agricultural water demands and its future prediction in Balkh Province using satellite remote sensing. In this study, a satellite-based evapotranspiration (*ET*) map estimated using the GCOM-C ET_{index} algorithm was integrated with a traditional method of calculating crop water requirements to understand the present status of agricultural water management in the Mazari-Sharif agricultural area. Landsat 8 images were used to analyze vegetation and water status for the year 2015. Using historical and future data sets, the impact of climate change on crop water requirements and irrigation water requirements were estimated to understand future conditions.

Keywords: Crop Water Requirements, Irrigation Water Requirements, Afghanistan, Remote-Sensing, Climate Change

1. Introduction

Afghanistan is located in an arid to semi-arid climate zone of Asia, with scarce rainfall. The rainy season starts in October and ends in April (Qureshi, 2002, and Gopal, 2003). The mountains in the country serve as a natural storage facility and a source of water for agricultural production. The mountains accumulate snow during winter, which starts melting in the spring season. Therefore, together with the melting of glaciers, the mountains feed rivers that are the main sources of surface water. This water is mainly used for agricultural production.

Aside from security and political stability, water is the most critical need for Afghanistan that can lead the country toward development sustainability and self-sufficiency. Based on a United Nations estimation, Afghanistan's population is 31 million, and it will increase by about 80 percent by the year 2050 to approximately 56 million (Campbell, 2015). This increase will strengthen water demand, which is already a problem for the country's water resources. Furthermore, recent studies show that climate change may increase air temperature and alter precipitation patterns in Afghanistan (WFP et al., 2016). Specifically, this change may affect the amount and timing of snowfall received in High Mountain, which significantly impacts the country's water resources.

At present, in addition to many ongoing water projects and the construction and modernization of irrigation systems, water is applied and distributed based on a traditional system without considering actual crop or irrigation requirements (Walters and Groninger, 2014).

Considering the above-mentioned problems, this study attempts to deliver a clear picture of agricultural water demands along with future predictions about conditions in Balkh Province for readers.

[1] University of Miyazaki (1-1, Gakuen Kibanadai-Nishi, Miyazaki 889-2192, Japan; E-mail: tasumi@cc.miyazaki-u.ac.jp)

2. Materials and Methods

Weather data and satellite Landsat images were the main sources used in this research. To understand the present conditions of agriculture water management in the Balkh agricultural area, a combination of a satellite-based *ET* map estimated by the GCOM-C ET_{index} algorithm (Tasumi et al., 2016 a,b) with the traditional technique of crop water requirement computation (Allen et al., 1998) was used.

For the year 2015, the actual *ET* was computed from Landsat 8 and crop water requirements were obtained from the FAO 56 manual. In the same year, the spatial results of field water sufficiency were derived, which show the adequacy of water in Balkh Province. The estimation of crop water requirements using FAO 56 require the crop coefficient curve and *ETo*. The K_c values were determined from the literature and from satellite-observed NDVI. Climate change impacts on CWR and IWR were computed using daily historical (1981–2015) and future (2016–2100) weather data. Historical weather data were used to confirm recent trends in field water demands, and future weather data were used to evaluate the impacts of climate change.

2-1. Study Area

Balkh is an agricultural province in northern Afghanistan, located at a latitude of 36.76°N, a longitude of 66.9°E, and 334 m in elevation above sea level (NAIS/AgNet, 2008). In Balkh Province, irrigated agricultural land covers 266,006 ha, which is equal to 15.9% of the whole province (FAO, 2016). The main sources of water to this region come from the Hindu Kush Mountains, flowing through the Balkhab River.

Balkh has an arid (desert) climate with a cold winter and a hot summer. The annual average rainfall is about 260 mm; most rain occurs from November to May, and very little rainfall occurs during summer. In this study, we focus on agricultural areas that cover an 83,090 ha

area.

Figure 1 shows the location, boundaries, and topographic map of the study area. The location and boundaries of the analysis areas used in this study are shown (black line) inside Balkh Province. The topographic map of the study area indicates that nearly half of the province has mountainous or semi-mountainous terrain. In this research, the flat land area was selected as a study area.

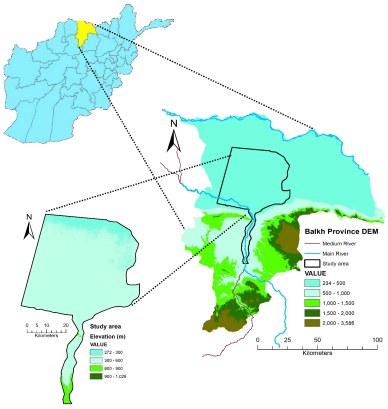

Figure1: Topographic and location map of study area

2-2. Weather data

Weather data is an important part of this research. Because climatic parameters are the only factors that affect *ETo*, weather data are used to compute *ETo*. In this study, *ETo* is calculated using the FAO's Penman–Monteith method (Allen et al., 1998).

Figure 2 shows the daily air temperature (top), computed *ET* (middle), and wind speed (bottom) for the year 2015. This figure shows the general weather conditions of Balkh Province during the year 2015.

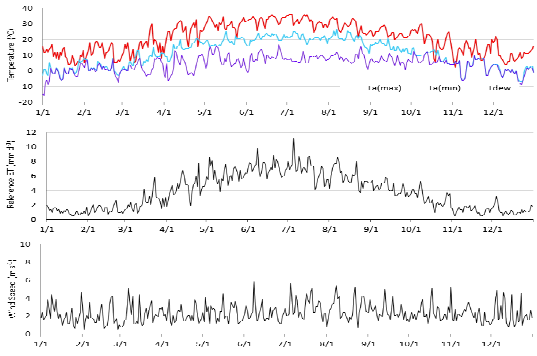

Figure 2: Daily plots of temperatures (top), computed reference *ET* (middle), and wind speed (bottom) for the year 2015

2-3. Satellite Landsat images analysis

The 2015 Landsat 8 images of Balkh were downloaded, and consist of two paths (154_155) and two rows (34_35). In total, 90 images from 2015 were downloaded. Same-day image rows (34_35) were merged together, resulting in 23 images from path 154 and 22 images from path 155.

In this study, band 10 (TIRS) was used to estimate *ET*, and band 4 (red) and band 5 (near-infrared) were used to estimate NDVI.

The ET_{index} is equivalent to the crop coefficient. It is an index defined by the FAO that is widely accepted in the field of agricultural water management. The following equation shows the estimation of the ET_{index}:

$$ET_{index} = ET/ETo \qquad (1)$$

where *ET* actual is from a hypothetical, adequately watered, extensive grass reference surface with a crop height of 12 cm, a surface resistance of 70 s m−1, and an albedo of 0.23. *ETo* is reference evapotranspiration, which can be calculated using meteorological data.

ET is estimated by applying the GCOM-C ET_{index} algorithm (Tasumi et al., 2016 a,b), which is a simplified *ET* estimation algorithm that has good congruency with traditional methods of agricultural water planning and management. The key equation of the algorithm is:

$$ETindex = Cadj \times \frac{Ts(dry) - Ts(act)}{Ts(dry) - Ts(wet)} \qquad (2)$$

where *Cadj* is an empirically determined adjustment factor, T_s(act) is the actual surface temperature (°C) observed via satellite, and T_s(wet) and T_s(dry) are the wet and dry surface temperatures (°C) estimated using clear-sky solar radiation and observed wind speed.

The estimated ET_{index} is further convertible to actual *ET* (mm/day), using reference evapotranspiration (*ETo*) as:

$$ET = ET_{index} \cdot ETo \qquad (10)$$

where *ETo* is reference evapotranspiration computed based on weather data.

Monthly and annual *ET* are both further estimated using the ET_{index} (satellite data) after interpolating cloudy days, and *ETo* (weather data).

2-4. Crop classification and crop water requirement

The crop classification was conducted in the Mazari-Sharif agricultural area using a series of NDVI images. For the identification of vegetated and non-vegetated surfaces, pixels with NDVI values consistently less than 0.3 were assumed to be non-crop surfaces, which are not targeted for crop classification. The remaining pixels were classified into 100 classes, using unsupervised classification based on the information from the NDVI time series (i.e., phenology). The 100 classes were then manually assigned to each crop type or non-crop categories, using general information about the primary crops and the cultivation schedule of the area. Upon classification, the following two pieces of information were used as references: (1) the crop calendar supplied by the National Agriculture Information System (NAIS)/AgNet for the year 2007 for Balkh/Dehdadi; and (2) the planting areas and harvesting period for Balkh, 2008, by NAIS/AgNet.

After a trial-and-error analysis, the crops were categorized into the following seven categories: winter wheat, spring wheat, first cultivation of winter wheat and then cultivation of cotton, first cultivation of spring wheat and then cultivation of cotton, other field crops, and horticulture (likely apricot).

Next, the crop water requirement for each crop-type was analyzed by following the FAO manual (Allen et al., 1998). The FAO suggests estimating crop water requirements by determining the crop coefficient curve.

In this study, the crop coefficient curve for each crop type was determined by referring to published values and the satellite-observed NDVI for crop phenology. Then, the crop water requirement for each crop type was computed using estimated *ETo* based on ground-measured weather data and the crop coefficient curve of that specific crop.

Finally, a field water sufficiency map was derived via dividing the actual satellite-estimated *ET* by crop water requirement, as estimated from the FAO manual.

2-5. Climate change impact on field crops and irrigation water requirements

The impact of climate change on agricultural water requirements was analyzed for the Mazari-Sharif agricultural area. The available data for this analysis were as follows:

1. Historical weather data (daily temperature and precipitation) (1986–2015)
2. Future weather data (daily temperature and precipitation) (2016–2100)

In this study, to analyze the impact of climate change on field crops, two climate change scenarios, RCP45 and RCP85, were used to evaluate the impact of climate change on the study region over time relative to the historical baseline conditions. From each of these scenarios, eight models were used to project future conditions, as well as one model for considering the historical conditions. The future period was set to 2016–2100, and the historical period was set to 1986–2015.

The analysis of IWR and CWR was based on the provided future data from the eight models of RCP45 and the eight models of RCP85, with one historical weather data set from ERAi.

The analysis of climate change impacts on field crops was conducted to evaluate long-term trend changes and the year-by-year variation of precipitation (Pr), crop water requirement (CWR), and irrigation water requirement (IWR) for spring wheat.

The long-term trend was evaluated as a linear regression that shows the general change of Pr, CWR, and IWR, and explains how climate change causes Pr, CWR, and IWR to increase or decrease.

3. Results and Discussions

3-1. Satellite analysis result for the year 2015

Figure 3 shows the key findings of the satellite application for the Mazari-Sharif agricultural area in the year 2015. These results are shown as summary images.

A summary of the description of each image in Figure 3 is as follows:

A: Annual actual evapotranspiration for the year 2015. This image is a valuable source for agricultural water management.

B: Crop classification map for the year 2015. This image can be used for many important purposes in the field of agriculture and irrigation planning.

C: Crop water requirements for classified crops in one season. This result is vital for planning agricultural water resources.

D: Field water sufficiency map for the year 2015. This result shows the present conditions of the study area and shows where water is insufficient.

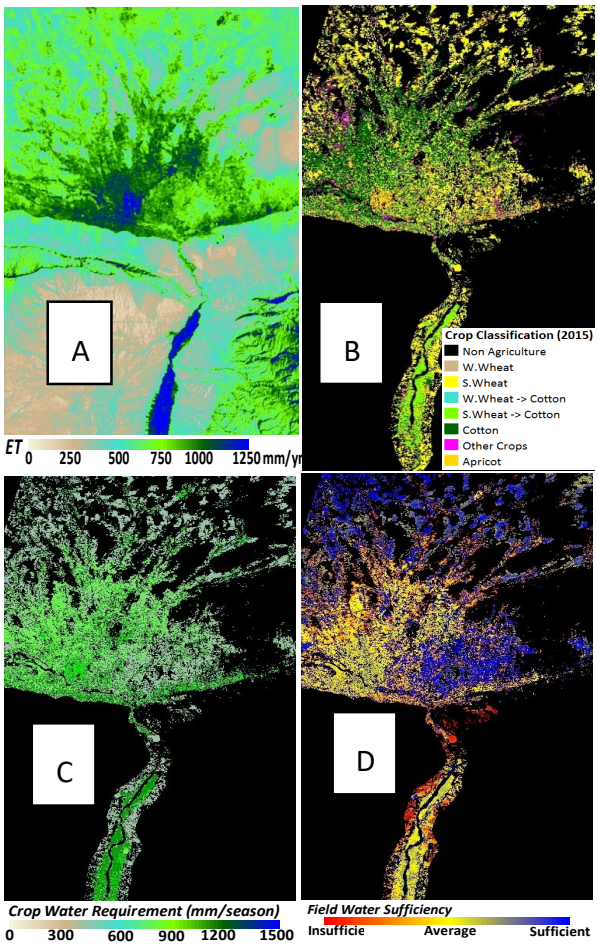

Figure 3: A: Estimated ET for the year 2015, B; Crop classification map for the year 2015, C; CWR for the cultivation season of 2015; and D: Field water sufficiency map for the year 2015.

3-2. Climate change impacts on field water requirements

The results of CWR and IWR are focused on the major crop of Balkh Province, which is spring wheat. The results also include the precipitation data.

The impact of climate change on CWR and IWR and precipitation are shown in Figure 4. These trends are present for all climate models, and for all precipitation, CWR, and IWR data. The graphs' trends in precipitation are summarized in Table 1, and the summary for annual variation of spring wheat CWR and IWR are shown in Table 2 and 3.

Figure 4 shows a sample result of climate change impact on irrigation water requirement from the RCP85 MPI-ESM-MR assumptions for spring wheat:

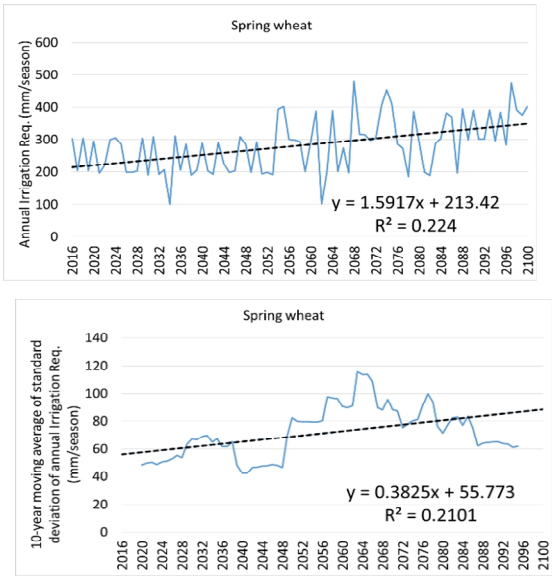

Figure 4: Annual irrigation water requirement (2016–2100) for spring wheat, and 10- year moving standard deviation of annual irrigation water requirement from the RCP85 MPI-ESM-MR assumption, Balkh Province

In Figure 4, (top) shows the annual IWR in the future, adopting the RCP85 MPI-ESM-MR scenario. In this scenario, the IWR has an increasing trend in the future, and the ratio of the increment is 1.6 mm/season. Furthermore, the standard deviation of the IWR (Fig. 4, bottom) indicates that the IWR becomes more unstable in the future, meaning that little water may be required in some years, whereas large amounts of water may be required in some other years. The average increment ratio of instability is about 0.4 mm/season. Because water planning should target years with water shortage, an unstable year-by-year IWR increases the water requirement in planning. A quick reference number of the impact of climate change on IWR, including the impact of the instability of water demand, may be 1.6 mm/season (i.e., the general ratio of increment) + 0.4 mm/season (impact of increment of instability) = 2 mm/season. Comparing the historical annual IWR of spring wheat (which is about 236 mm/season), a 2 mm/season increment of IWR is equivalent to a 42% increment of IWR in 50 years, which is large. One important caution regarding this analysis is that the R-square values are very small for both the IWR and the trend in standard deviation. The small R-square values imply that the above-mentioned trend is unclear or uncertain. This analysis assumes fixed soil and crop conditions. Thus, the trend of IWR shown in Fig. 4 is a pure reflection of the trend of climatic conditions described by the climate change model.

3-2-1. Summary table for the result of precipitation

The results of the analysis of climate change impact on field water requirement are described in a summary table. The data period is 2016–2100 for the future, and 1981–2015 for historical ERAi data.

As shown in Table 1, the first model is "CanESM2", which lists the annual amount and 10-year standard deviation in the same way: both show the average (mm/year), slope, and R-square values. In the annual amount section, the average amount is 194 mm/year, which represents the average of the annual precipitation from 2016–2100. The slope is 0.75, meaning that the annual precipitation trend has an increment of 0.75 mm/year. However, the R-square value is 0.05, which indicates that the increment is not clear. Thus, with a small R-square value, the model should be considered as an unclear predictor. In the 10-year standard deviation section, the average is 80 mm/year, which indicates the average of yearly variation for the entire period (2016–2100). The slope is 0.28, which means that the year-to-year variation trend has an increment of 0.28 mm/year, although the R-square value of 0.13 indicates that it is also not a significant, clear predictor.

Table 1: Summary of annual precipitation: long-term and year-by-year variation

Percipitation	Annual amount			10-year Standard deviation		
Model name	Average (mm/yr)	Slope	R^2	Average (mm/yr)	Slope	R^2
CanESM2_rcp85	194	0.75	0.05	80	0.28	0.13
CNRM-CM5_rcp85	182	0.55	0.08	44	0.05	0.01
MPI-ESM-MR_rcp45	166	0.11	0.00	48	0.21	0.29
CCSM4_rcp45	160	0.10	0.00	51	0.26	0.12
CNRM-CM5_rcp45	181	-0.06	0.00	42	-0.08	0.05
CanESM2_rcp45	171	-0.08	0.00	73	0.49	0.15
NorESM1_rcp85	136	-0.11	0.00	51	0.23	0.16
CCSM4_rcp85	180	-0.12	0.00	57	0.03	0.01
MIROC-ESM-CHEM_rcp45	158	-0.13	0.01	42	-0.03	0.01
GFDL-ESM2M_rcp85	137	-0.14	0.00	64	-0.18	0.06
NorESM1_rcp45	148	-0.22	0.01	49	-0.22	0.17
IPSL-CM5A-LR_rcp85	130	-0.36	0.02	59	0.01	0.00
IPSL-CM5A-LR_rcp45	135	-0.38	0.02	64	-0.18	0.08
MIROC-ESM-CHEM_rcp85	143	-0.43	0.05	41	-0.05	0.02
MPI-ESM-MR_rcp85	174	-0.47	0.06	47	0.24	0.14
GFDL-ESM2M_rcp45	168	-0.67	0.06	62	-0.06	0.01
ERAi	156	0.41	0.01	43	-0.07	0.01

Based on the summarized Table 1, 12 out of the 16 models (75 percent) have a negative slope, which indicates a decrease in future precipitation amount, whereas four models have a positive slope. In both cases, the R-square values of the models are not very large, or are close to zero, meaning that the given statistics or outcome of the regression line, which shows the decrease or increase, do not fit significantly and cannot be predicted. In the case of the 10-year moving average outcome, 37% of climate models indicate that the yearly variation of precipitation will decrease, meaning that in future, the precipitation amount is expected to be more stable year-by-year, whereas 62% of the models predict an increase in the year-by-year variation of precipitation. However, in both cases, the R-square does not agree compellingly with the outcome of the trend. Accordingly, the climate model outcomes clarify that precipitation and year-by-year variation may not go in one direction. Therefore, a good interpretation of the results is "no clear trend or direction" that could significantly predict the future precipitation conditions.

3-2-1. Summary table for the result of spring wheat crop water requirement and irrigation water requirement

In spring wheat CWR, all climate models have a positive slope, meaning that all models predicted an increase in demand in the future. Likewise, the R-square values are compatible with the slope; in other words, models with a higher slopes had a higher R-square values, or as the slope decreases, the R-square value goes down. The slope trends of the RCP85 models are more compelling than those of the RCP45 models. The highest increment among the models is 1.54 mm/season (Table 2). Thus, depending on the specific model, it is expected that spring wheat CWR will increase 1.54 mm/season every year in the future. In 10 years, this increment (spring wheat CWR) may increase to 15 mm/season, which is a 3–4% increase over the present amount. Concerning the year-to-year variation, 56% of climate models predicted that it will increase in the future, whereas 43% of models gave the opposite prediction. There was no clear agreement of direction among the models. The increment of year-by-year variation increases water demand, although the intensity of the increment (i.e., magnitude of the slope) is not very large.

The overall outcome for IWR for spring wheat is similar to spring wheat CWR. The visible differences in the seasonal trends of the amount of increment or decrement from each climate model (Table 3).

Table 2: Summary of seasonal CWR for spring wheat: long-term trend and year-by-year variation

Spring wheat, CWR	Annual amount			10-year Standard deviation		
Model name	Average (mm/season)	Slope	R^2	Average (mm/season)	Slope	R^2
MIROC-ESM-CHEM_rcp85	466	1.54	0.57	32	0.06	0.05
IPSL-CM5A-LR_rcp85	472	1.48	0.50	37	0.25	0.59
MPI-ESM-MR_rcp85	438	1.14	0.46	31	0.20	0.40
CanESM2_rcp85	454	1.04	0.40	31	-0.05	0.04
NorESM1_rcp85	452	1.02	0.38	31	0.02	0.01
CCSM4_rcp85	430	0.74	0.32	26	-0.07	0.05
IPSL-CM5A-LR_rcp45	447	0.64	0.21	32	0.14	0.20
NorESM1_rcp45	432	0.57	0.16	32	-0.14	0.28
CanESM2_rcp45	434	0.52	0.15	30	0.19	0.17
GFDL-ESM2M_rcp85	426	0.49	0.18	26	-0.08	0.09
MIROC-ESM-CHEM_rcp45	430	0.47	0.13	30	-0.01	0.00
GFDL-ESM2M_rcp45	409	0.33	0.08	29	-0.04	0.02
CCSM4_rcp45	424	0.30	0.09	23	-0.06	0.04
MPI-ESM-MR_rcp45	418	0.25	0.04	30	0.07	0.03
CNRM-CM5_rcp45	405	0.22	0.03	29	0.14	0.27
CNRM-CM5_rcp85	406	0.11	0.01	26	0.03	0.03
ERAi	379	0.72	0.06	31	0.20	0.06

Table 3: Summary of seasonal IR for spring wheat: long-term trend and year-by-year variation

Spring wheat, IR	Annual amount			10-year Standard deviation		
Model name	Average (mm/season)	Slope	R^2	Average (mm/season)	Slope	R^2
MIROC-ESM-CHEM_rcp85	316	1.92	0.34	63	0.27	0.20
IPSL-CM5A-LR_rcp85	339	1.72	0.22	82	0.38	0.34
MPI-ESM-MR_rcp85	282	1.59	0.22	72	0.38	0.21
NorESM1_rcp85	303	1.16	0.13	71	0.27	0.12
CanESM2_rcp85	296	1.06	0.10	75	0.13	0.05
CCSM4_rcp85	280	0.92	0.10	71	-0.09	0.02
GFDL-ESM2M_rcp85	286	0.86	0.08	73	-0.20	0.04
GFDL-ESM2M_rcp45	253	0.70	0.05	77	0.11	0.02
CanESM2_rcp45	276	0.60	0.03	77	0.68	0.35
NorESM1_rcp45	274	0.54	0.03	73	-0.28	0.09
IPSL-CM5A-LR_rcp45	321	0.45	0.02	71	0.45	0.32
CNRM-CM5_rcp45	240	0.30	0.01	63	0.21	0.39
MIROC-ESM-CHEM_rcp45	278	0.25	0.01	74	0.01	0.00
CCSM4_rcp45	283	0.20	0.01	61	-0.32	0.32
MPI-ESM-MR_rcp45	262	0.05	0.00	67	0.10	0.02
CNRM-CM5_rcp85	253	-0.20	0.01	60	-0.01	0.00
ERAi	236	1.24	0.03	70	0.40	0.14

4. Conclusions

Satellite remote sensing outcomes determine the present conditions of field water sufficiency as a spatial map; thus, to further improve agricultural products, it is recommended that this kind of research is extended to other areas. Of course, consideration and acknowledgment of the results of this kind of study are helpful when deciding to construct irrigation facilities.

Several climate model outcomes show that air temperature is increasing and precipitation is decreasing in the long-term future, which leads to an increment in crop and irrigation water requirements. The vast impacts of climate change, such as decreased rainfall and increased temperature, are visible in rainfed areas; therefore, the best solution is to change rain-fed agriculture into irrigated agriculture.

Acknowledgments

This study was conducted as a part of a World Bank Project “Pilot Climate Change Impact Analysis on Hydrology and Agriculture in Afghanistan (P160070)”, with partial collaborative support by the Promotion and Enhancement of the Afghan Capacity for Effective Development (PEACE) Project of Japan International Cooperation Agency (JICA). Authors acknowledge the technical advises and the assistances by the World Bank team, Dr. Toru Konishi, Dr. Thomas Mosier, Dr. Hiroaki Somura, Mr. Shoaib Saboory, and Mr. Ezatullah Rabanizada.

References

1) Allen, R. G., Pereira, L. S., Raes, D., and Smith, M., 1998. Crop Evapotranspiration: Guidelines for computing crop water requirements. FAO Irrigation and Drainage Paper 56. FAO, Rome, Italy, p. 300.

2) Campbell, J., 2015. A dry and ravaged land: Investigating water resources in Afghanistan. Retrieved from http://www.earthmagazine.org

3) FAO, 2016. The Islamic Republic of AFGHANISTAN Land Cover ATLAS, http://www.fao.org/3/a-i5043e.pdf.

4) Gopal, B., 2003. Aquatic biodiversity in arid and semi-arid zones of Asia and water management (pp. 199–216). Kluwer Academic Publishers: Norwell.

5) National agriculture information system (NAIS)/AgNet for the Afghan Ministry of Agriculture, Irrigation and Livestock (MAIL), 2008. Accelerating sustainable agriculture program. *Balkh Agricultural Profile.*

6) Qureshi, A.S., 2002. Water resources management in Afghanistan: The issues and options (Vol. 49). International Water Management Institute.

7) Tasumi, M., Kimura, R., Allen, R.G., Moriyama, M. and Trezza, R., 2016a. Development of the GCOMC global ETindex estimation algorithm. *Journal of Agricultural Meteorology 72*, pp. 85–94.

8) Tasumi, M., Moriyama, M., Hirakawa, K. and Fujii, A., 2016b. Evaluation of the GCOM-C global ETindex estimation algorithm. *Journal of Agricultural Meteorology 72*, pp. 151–158.

9) Walters, S.A. and Groninger, J.W., 2014. Water distribution systems and on-farm irrigation practices: Limitations and consequences for Afghanistan’s agricultural productivity. *Water International, 39*(3), pp. 348–359.

10) WFP, UNEP and NEPA, 2016. Climate change in Afghanistan

Classification of soil at subgroup level and its digital mapping in the Khost Province of Afghanistan

○Emal Wali [1], Masahiro Tasumi [1], Yoshinori Shinohara [1]

Abstract: In this study, we developed a digital soil map for the Khost Province of Afghanistan. The developed map contains soil taxonomic information up to subgroup level. We collected two times soil samples from 64 and 50 locations in and around the Khost Province through an intensive soil survey. First, we classified the soils of Khost province into 14 subgroups of soils, following the USDA soil classification system. Secondly, we used a Soil Land Inference Model (SoLIM) to map the recognized 14 soil subgroups digitally, via an expert knowledge-based fuzzy soil inference scheme, as surface topography and other spatial data i.e. soil depth, rainfall, geology map and soil great groups. Finally, we used the 50 soil samples for the accuracy assessment. The overall accuracy from the error matrix and Kappa statistics is 0.74 and 0.711 respectively. The developed map could be useful for advanced usage of soil information, for instance to better determine the crop type for cultivation considering the detailed soil properties.

Keywords: *Soil subgroup; SoLIM; Soil classification; Digital soil mapping*

1. Introduction

Soil classification is fundamental for effective use of soil resources including for food production and ultimately food security, generating bio-products, advancing the biodiversity conservation, and guaranteeing environmental wellbeing (Boonsompopphan et al. 2008). Detailed soil attributes and spatial information is useful for many environmental modeling and land management applications (Burrough 1996; Corwin, Vaughan, and Loague 1997; Stehfest et al. 2014; Borrelli et al. 2014; Panagos et al. 2016). Also, as summarized by (Eswaran et al. 2002), soil classification is important not only for soil sciences, but also for many other natural, social, economic, cultural, and technical sciences.

Soil classification regards as essential information; therefore, soil maps have been developed in almost all developed regions of the world. As a popular classification method, the United States Department of Agriculture (USDA) suggests a hierarchical soil taxonomy classification system (USDA-NRCS, 2014 and USDA-SCS, 1975), classifying soils from “Order”, “Suborder”, “Great group”, “Subgroup”, “Family”, to “Series” levels.

In Afghanistan, the Institute of Applied Botany of Leningrad examined soil characteristics in 1924 and 1926–1927. The institute collected few soil samples and conducted physical and chemical analyses. Based on their observations, the soils were classified into four groups: 1) Heavy Loam spread in low river valleys, 2) Loess-like Loam spread in the foothills in northern Afghanistan, 3) Medium Loams spread in sloping surfaces, and 4) the cultivated–irrigated soils in the oases and urban centers (Hildreth 1957). (Salem and Hole 1969) conducted a more detailed research on Afghan soil properties and classification. They studied eight pedons in the country and found that most of the soils in these areas were classified as Aridisols and Entisols. The latest soil map of Afghanistan (Shroder 2014) contains only 25 soil regions that are defined based on soil great groups, soil moisture, and temperature regimes by the United States Department of Agriculture–Natural Resources Conservation Service (USDA-NRCS) in 2001. Under this classification, the soils of the study area comprise five soil regions and six great soil groups. In general, soil taxonomy classifies the soil based on “family” or its smallest unit, “series level.” The soils of the US and most parts of Thailand are classified up to the series level. Compared to these examples, the currently available soil map of Afghanistan (e.g., classify up to great group level) is insufficient, with limited soil information. Achieving more detailed soil classification allows Afghanistan farmers to use the soil resources more effectively, such as to better determine the crop type to cultivate considering the detailed soil properties.

This study aimed to develop an advanced soil map for the Khost Province of Afghanistan. As the first attempt, to the best of our knowledge, in the country, soils are classified at the subgroup level, following the USDA soil classification system, and the

[1] University of Miyazaki (1-1, Gakuen Kibanadai-Nishi, Miyazaki 889-2192, Japan; E-mail: tasumi@cc.miyazaki-u.ac.jp)

result of classification is expressed as a digital soil map. A well-developed and systematic digital soil map can help the farmers of the Khost Province to achieve higher yields and cultivate different types of crops in their respective farms.

2. Methods and Materials

2.1. Study area

The Khost Province is located in the Southeastern part of Afghanistan. Its land area has a trapezoidal shape with a maximum length of approximately 100 km in the east-west direction with a maximum width of approximately 60 km. The province lies at a base elevation of approximately 1,180 m above sea level and it is located between 33° 59′, 33° 46′ North latitudes, 69° 19′, and 70° 21′ East longitudes. The province has a land area of 4131.8 km^2. Figure 1 shows the location and the elevation distribution of the province. High mountains are spread in the west part of the province. Flat or semi-flat areas are located in the central and the eastern regions of the province. More than 50% of the soils have a pH between 8 and 8.5, approximately 35% of the soils have a pH between 8.5 and 9, and 10% of the soils have a pH of 9 and above (FAO/UNDP 1973).

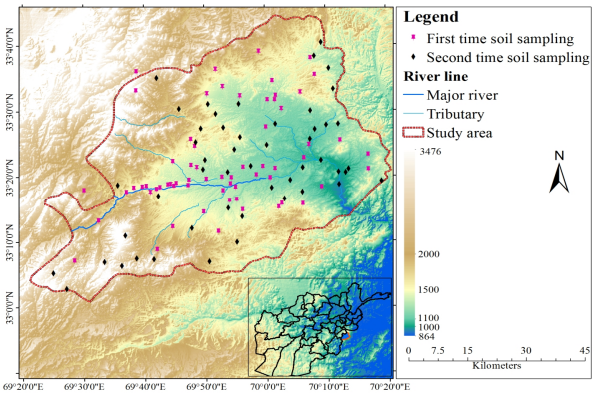

Figure 1: Geographical location of the Khost Province in Afghanistan and the location of soil sampling sites.

(Hashami 2011) studied six soils in the Khost Province, and concluded that the soils in the region varied in their initial phosphorus and zinc contents and many other soil properties. In the Khost Province of southeastern Afghanistan, most of the farmers grow wheat (*Triticum aestivum L.*), maize (*Zea mays L.*), rice (*Oryza sativa L.*), clover (*Trifolium sp.*), and mung bean (*Vigna radiata [L.] R. Wilczek*). Wheat is mainly planted in autumn (mid-October), whereas maize and rice are planted during the beginning of the summer season (mid-June to mid-July) (Wali et al. 2016).

2.2. Methodological framework

The soil mapping process is divided into three phases. The procedure is abstracted in Figure 2.

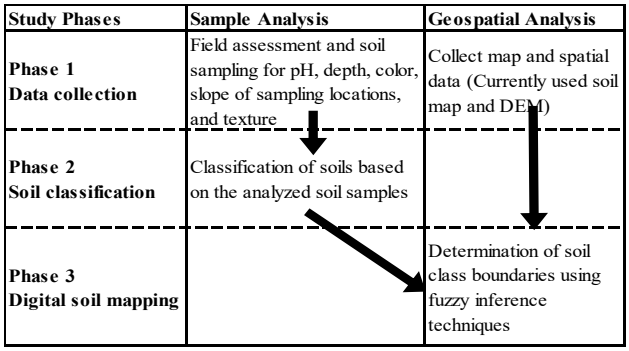

Figure 2: Schematic chart of materials and methodologies applied for digital soil map production

As the first phase, necessary data and information are collected. As the second phase, soils are classified based on the information from soil sample analyses. Finally, as the third phase, a digital soil map is created by geospatial analysis using the results from the analyses in phase two and surface topography and other spatial data as inputs.

2.2.1. Data collection

Two times soil surveys were conducted in the Khost Province in 2016 and 2017. Information for pH, soil depth, soil color, and soil texture classes were obtained for 64 and 50 locations in and around the province respectively. The first time soil survey information were used to classify and digitally map soils in the Province, while the second time soil survey information were used to perform the accuracy assessment. The sample locations are indicated in Figure 1. The first time soil sample locations were determined by considering the spatial distribution of the sample locations, convenience in access, and by considering the land-use map published by the FAO, while the second time samples were collected considering a pre-designed stratified random sampling. The developed digital soil map was converted to a thematic map in ArcGIS and the stratified random sampling was performed in ERDAS Imagine software. As the secondary data, the map of the great soil groups produced in 2001 by the USDA-NRCS, Soil Science Division (Figure 3), geology map produced by USGS and the GIS and Statistics Department of the Ministry of Agriculture, Irrigation and Livestock (MAIL), Afghanistan, granted DEM at 10-m resolution. The data for rainfall was derived from the daily weather data produced by NASA Prediction of Worldwide Energy Resource (POWER).

2.2.2. Soil classification

The 64 soil samples obtained during the field observations were classified according to the USDA diagnostic procedure as described in the manuals (USDA-NRCS, 2014 and USDA-SCS, 1975). The classification system we adopted in this study is a hierarchical system of soil classification that has many levels. In this study, we aimed to classify soils up to the more detailed "subgroup" level. Soils should be classified by their own properties and the taxa defined strictly by the soil properties (USDA-SCS, 1975). For soil properties, this study adopted soil color, soil pH, soil depth, slope, and soil textural classes, which is the typical set of soil properties used for this type of classification. The classified subgroups of soils are then appropriately named by referring to the manual. The USDA soil taxonomy classification system is not a pure mechanical process but requires some specialist decisions on some details. In this study, classification is conducted by consulting with 10 local soil scientists.

2.2.3. Digital soil mapping

Once the 64 soil samples were classified and named, the next step was mapping. During the mapping process, the soil classification boundaries were determined and delineated. There are two different methods of soil mapping. One is the conventional soil mapping, where the soil surveyor classifies soil samples and manually determines the boundaries of soil classes, with the help of the topographic information obtained through a stereoscopic survey using aerial photographs. The other method is the digital soil mapping (A Xing Zhu et al. 2001). This study adopts the digital soil mapping, because the method is thought to be more up-to-date and an accurate procedure compared to the conventional method. As an additional advantage of the digital soil mapping method, the minimum requirement of input data is limited so that the method is applicable even for the places where the ground information is limited. A software program called "SoLIM " (A Xing Zhu and Band 1994; A Xing Zhu et al. 1996; A Xing Zhu 1997; A X Zhu et al. 1997; A Xing Zhu 2000) was applied to create a digital soil map of the study area. SoLIM incorporate a soil-land inference model designed to address the limitations of the conventional soil survey. This approach combines the knowledge of local soil scientists with GIS techniques under fuzzy logic to map soils (A Xing Zhu et al. 2001). (A Xing Zhu and Band 1994; A Xing Zhu et al. 1996; A Xing Zhu 1997), conducted studies to derive soil similarity vectors based on the classic concept of (Jenny 1980; Jenny Hans 1994) that there exist relationships between soils and their formative environments. They used geographic information processing techniques to characterize the soil formative environments and developed a set of knowledge acquisition techniques to capture the relationship between soils and their formative environments from a soil scientist. A set of fuzzy inference techniques called a "fuzzy inference engine" was used to integrate the soil formative environments into a geographic information system (GIS) with the soil environment relationship to derive soil similarity vectors over the area. In this study, the following nine environmental variables were used as the input data to characterize the soil formative environments according to (A Xing Zhu et al. 1996): Spatial distribution of soil depth, spatial distribution of rainfall, geology map of Afghanistan, soil great groups, surface elevation; surface slope, aspect of the surface, flow direction; and the land curvature information. (A Xing Zhu et al. 1996) noted that two types of information, 1) where a soil class typically occurs in terms of environmental conditions and 2) the response of a soil class to variation in the environmental conditions is needed to analyze the relationships between soil distribution and its environmental conditions. Both types of information had to be extracted from local soil experts. In this study, this information was obtained by interviewing the 10 local soil scientists who had participated during the soil classification procedure.

Once the data of the environmental variables were prepared and the relationships between soil distribution and its environmental conditions were analyzed, the fuzzy inference engine was used to compare each of the similarity values for the soil at a location to each of the prescribed subgroups of the soil.

3. Results and discussion

This study has two major outcomes. The first outcome is the classification results from the 64 soil sample locations, considering the five major soil properties (i.e., soil pH, soil depth, soil color, surface slope, and soil texture). This result determines all of the available soil classes in the Khost Province. The second outcome is the digital soil map using the SoLIM software.

3.1 Soil classification outcome

In soil classification, first, the 64 soil samples were categorized into 14 soil subgroups, considering the soil properties. The criteria used were recommended by the local soil scientist, with reference to the manual

(USDA-NRCS, 2014 and USDA-SCS, 1975). The resulting list of soil classes for the Khost Province is summarized in Table 1, with the sample numbers.

Table 1: Recognized soil subgroups in the study area

No	Classified Soils	No. of Soil Samples
1	Anthropic Torrifluvents	2
2	Aquic Torrifluvents	2
3	Aquic Torriorthents	5
4	Aquic Xerorthents	3
5	Calcixerollic Xerochrepts,	1
6	Haplocambids with Torriorthents	8
7	Lithic Haplocambids	8
8	Lithic Torriorthents	2
9	Rocky Land with Lithic Haplocambids	8
10	Typic Torrifluvents	3
11	Typic Torripsamments	7
12	Typic Xerorthents	2
13	Ustic Torrifluvents	6
14	Vitrixerandic Torrifluvents	7
	Total	64

The resulting number of classes was 14, indicating that the soil map, developed through this study will provide much more detailed information if compared to the currently available information (i.e., six classes of soil great groups as shown in Figure 3).

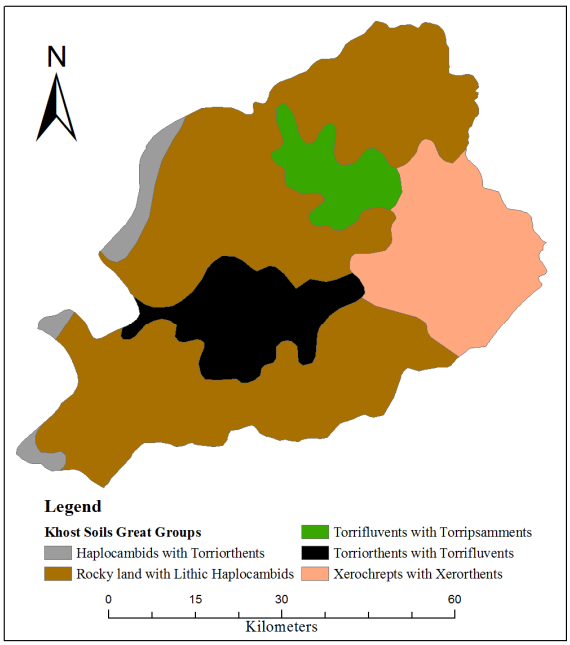

Figure 3: Spatial distribution of soil great groups in Khost Province. This map is reproduced and re-projected from the original map produced by USDA-NRCS in 2001.

As a limitation of this study, the number of soil samples is insufficient to describe the soil distribution perfectly in the region. Owing to the difficulty of increasing the sampling number, we carefully determined the soil sampling locations. However, the possibility of a class having a very small sample number (e.g., one or two samples per class) implies the instability of the determination of the class. For example, without the availability of one soil sample, which was categorized as "Calcixerollic Xerochrepts," we do not recognize the occurrence of the soil class in the entire province.

3.2 Digital soil mapping outcome

The results of digital soil mapping are presented in Figure 4. As a limitation of this study, it was not possible to collect more than 50 soil samples for the accuracy assessment due to the strict restrictions in sampling numbers. For discussing the performance of the developed map, an error matrix (Table 2) and Kappa statistics was considered to compare the resulting map (Figure 4) with new soil information came from the 50 more soil samples.

An error matrix is a square array of numbers placed in rows and columns. It shows the number of sample units i.e. pixels, clusters of pixels assigned to a particular category relative to the actual category as verified on the ground (Congalton 1991). Kappa is another discrete multivariate technique used for accuracy assessment (Congalton 1991). The Kappa statistics can be computed from the following equation originally published in (Bishop, Fienberg, and Holland 1975).

$$\hat{K} = \frac{N\sum_{i=1}^{r} x_{ii} - \sum_{i=1}^{r}(x_{i+} * x_{+i})}{N^2 - \sum_{i=1}^{r}(x_{i+} * x_{+i})} \qquad (1)$$

Where r is the number of rows in the matrix (Table 4), x_{ii} is the number of observations in row i and column i, x_{i+} and x_{+i} are the marginal totals of row i and column i respectively, and N is the total number of observations (Bishop, Fienberg, and Holland 1975).

In this study, the overall accuracy from the error matrix and Kappa statistics is 0.74 and 0.711 respectively. Moreover, the error matrix (Table 2) also represent the accuracy of each category separately. The total number of correct pixels in a category is divided by the total number of pixels of that category, derived from the reference data. (Congalton 1991) stated that the accuracy results indicates the probability of a reference pixels being correctly classified. This accuracy measure is often called "producer's accuracy" because the producer of the classification is interested in how well a certain class can

be classified. On the contrary, if the total number of correct pixels in a category is divided by the total number of pixels that were classified in that category, the results is a measure of commission error. This measure is also called “user accuracy”. The user accuracy indicates the probability of a pixel classified on the map/image actually represent that category on the ground (Congalton 1991). The error matrix and Kappa statistics tells us that there is 74 % and 71 % agreement between the classified data and reference data.

Table 2: Summary of Accuracy assessment. The numbers 1-14 represent each soil classes, columns represent the reference data, and the rows represent the classified data

Soils	1	2	3	4	5	6	7	8	9	10	11	12	13	14	Row total	Producer's accuracy (%)	User's accuracy (%)
1	2						1								3	100	66.67
2		2													2	100	100
3			2				1								3	66.67	66.67
4				2				1							3	100	66.67
5		1			1										2	100	50
6						5			1						6	83.33	83.33
7							4							1	5	57.14	80
8								2							2	66.67	100
9						1			8			1			10	80	80
10								1	1						2	100	50
11							1			2					3	100	66.67
12												2	1		3	50	66.67
13												1	3		4	50	75
14													1	1	2	100	50
Column total	2	2	3	2	1	6	7	3	10	1	2	4	6	1	50		

Overall Classification Accuracy = 37/50 = 74 %

(Taghizadeh-Mehrjardi et al. 2014) conducted similar study to map great soil groups. Their model predicted six great soil groups with over all accuracy of 67.5 %.

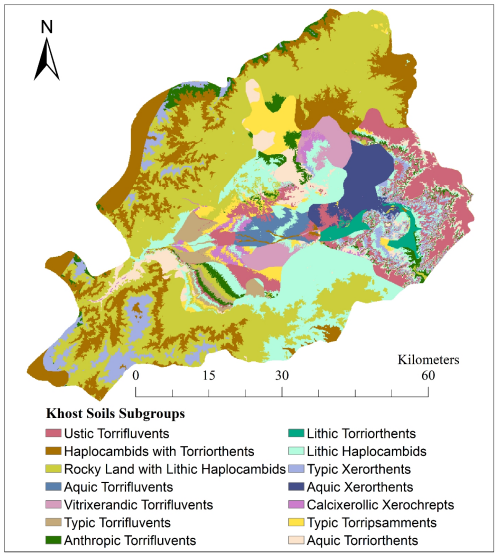

Figure 4: Spatial distribution of soil subgroups in the study area

4. Conclusions

In this study, we developed a digital soil map for the Khost Province of Afghanistan. The developed map contains soil taxonomic information up to the subgroup level, which is the first attempt in Afghanistan. Soil samples were collected from 64 and 50 locations in and around the Khost Province through an intensive soil survey. The collected samples were classified into 14 soil subgroups following the USDA soil classification system, considering the soil properties, which are soil depth, soil color, and slope of the surface, soil texture, and soil pH. As the classification system is not a pure mechanical procedure but requires expert decision for some detailed cases, the classification process was performed with the consultation of 10 local soil scientists. Once the soil classification was completed, a Soil Land Inference Model (SoLIM) was applied for mapping the recognized 14 soil subgroups digitally, via an expert knowledge-based fuzzy soil inference scheme, as surface topography and other spatial data as inputs. Our results showed that the soils of the Khost Province have 14 different classes of soil subgroups under the USDA soil classification system. As a limitation of this study, it was not possible to collect more than 50 soil samples for the accuracy assessment due to the strict restrictions in sampling numbers. Using the 50 samples the overall accuracy from error matrix wax 0.74 with a Kappa statistics 0.711. The findings of this study would enable the government of Afghanistan to devise suitable mechanisms to facilitate and promote the adoption of digital soil mapping of the whole territory of Afghanistan through policy formulation and implementation.

References

Bishop, Y M M, S E Fienberg, and P W Holland. 1975. “Discrete Multivariate Analysis: Theory and practiceMIT Press.” *Cambridge, Massachusetts*.

Boonsompopphan, Buree, Taweesak Vearasilp, Russell S Yost, and Tasnee Attanandana. 2008. “Field Identification of Soil Series: Indexing and Retrieving Soil Information While Sharing Experience and Knowledge.” *Soil Science* 173 (10): 736–44.

Borrelli, P, P Panagos, C Ballabio, E Lugato, M Weynants, and L Montanarella. 2014. “Towards a Pan-European Assessment of Land Susceptibility to Wind Erosion.” *Land Degradation and Development*. doi:10.1002/ldr.2318.

Burrough, Peter A. 1996. “Opportunities and Limitations of GIS-Based Modeling of Solute Transport at the

Regional Scale." *Applications of GIS to the Modeling of Non-Point Source Pollutants in the Vadose Zone*, no. applicationsofg: 19–38.

Congalton, Russell G. 1991. "A Review of Assessing the Accuracy of Classifications of Remotely Sensed Data." *Remote Sensing of Environment* 37 (1). Elsevier: 35–46. doi:10.1016/0034-4257(91)90048-B.

Corwin, Dennis L, Peter J Vaughan, and Keith Loague. 1997. "Modeling Nonpoint Source Pollutants in the Vadose Zone with GIS." *Environmental Science & Technology* 31 (8): 2157–75.

Eswaran, Hari, Robert Ahrens, Thomas J Rice, and Bobby A Stewart. 2002. *Soil Classification: A Global Desk Reference*. Boca Raton, Florida: CRC Press.

FAO/UNDP. 1973. *Calcareous Soils: Regional Seminar on Reclamation and Management of Calcareous Soils*. Cairo, Egypt: FAO/UNDP. https://books.google.co.jp/books?id=U8QOjwEACAAJ.

Hashami, Sayed Ziauddin. 2011. *Phosphorus and Zinc Availability in Selected Calcareous Soils from the Khost Province of Afghanistan*. Purdue University.

Hildreth, A C. 1957. *Afghan Soils in Relation to Agricultural Production*. Cheyenne, Wyoming.

Jenny, Hans. 1980. *The Soil Resource: Origin and Behaviour. Ecological Studies. Ecological Studies 37*. doi:10.1002/esp.3290070309.

Jenny Hans. 1994. *Factors of Soil Formation: A System of Quantitative Pedology*. New York: McGraw-Hill.

Panagos, Panos, Imeson Anton, Meusburger Katrin, Borrelli Pasquale, Poesen Jean, and Alewell Christine. 2016. "Soil Conservation in Europe: Wish or Reality?" *Land Degradation & Development* 27 (6): 1547–51.

Salem, M Zarif, and Francis D Hole. 1969. "SOIL GEOGRAPHY AND FACTORS OF SOIL FORMATION IN AFGHANISTAN." *Soil Science* 107 (4): 289–95. http://journals.lww.com/soilsci/Fulltext/1969/04000/SOIL_GEOGRAPHY_AND_FACTORS_OF_SOIL_FORMATION_IN.9.aspx.

Shroder, J F. 2014. *Natural Resources in Afghanistan: Geographic and Geologic Perspectives on Centuries of Conflict*. Elsevier Science. https://books.google.co.jp/books?id=2eNuAwAAQBAJ.

Stehfest, E, D van Vuuren, T Kram, L Bouwman, R Alkemade, M Bakkenes, H Biemans, et al. 2014. *Integrated Assessment of Global Environmental Change with IMAGE 3.0. Model Description and Policy Applications*. PBL Netherlands Environmental Assessment Agency: The Hague.

Taghizadeh-Mehrjardi, R., F. Sarmadian, B. Minasny, J. Triantafilis, and M. Omid. 2014. "Digital Mapping of Soil Classes Using Decision Tree and Auxiliary Data in the Ardakan Region, Iran." *Arid Land Research and Management* 28 (2). Taylor & Francis Group : 147–68. doi:10.1080/15324982.2013.828801.

(USDA-SCS) United States Department of Agriculture-Soil Conservation Services. 1975. Soil taxonomy: A basic system of soil classification for making and interpreting soil surveys-soil survey staff. Washington, DC.

(USDA-NRCS) United States Department of Agriculture-Natural Resources Conservation services. 2014. Keys to soil taxonomy, 12th ed. U.S. Government Printing Office, Washington, D.C.

Wali, Emal, Avishek Datta, Rajendra P Shrestha, and Sangam Shrestha. 2016. "Development of a Land Suitability Model for Saffron (Crocus Sativus L.) Cultivation in Khost Province of Afghanistan Using GIS and AHP Techniques." *Archives of Agronomy and Soil Science* 62 (7): 921–34.

Zhu, A X, Lawrence Band, Robert Vertessy, and Barry Dutton. 1997. "Derivation of Soil Properties Using a Soil Land Inference Model (SoLIM)." *Soil Science Society of America Journal* 61 (2): 523–33.

Zhu, A Xing. 1997. "A Similarity Model for Representing Soil Spatial Information." *Geoderma* 77 (2–4): 217–42.

Zhu, A Xing. 2000. "Mapping Soil Landscape as Spatial Continua: The Neural Network Approach." *Water Resources Research* 36 (3): 663–77.

Zhu, A Xing, and Lawrence E Band. 1994. "A Knowledge-Based Approach to Data Integration for Soil Mapping." *Canadian Journal of Remote Sensing* 20 (4): 408–18.

Zhu, A Xing, Lawrence E Band, Barry Dutton, and Thomas J Nimlos. 1996. "Automated Soil Inference under Fuzzy Logic." *Ecological Modelling* 90 (2): 123–45.

Zhu, A Xing, B Hudson, J Burt, K Lubich, and D Simonson. 2001. "Soil Mapping Using GIS, Expert Knowledge, and Fuzzy Logic." *Soil Science Society of America Journal* 65 (5): 1463–72.

森林における GCOM-C 蒸発散指数推定アルゴリズムの精度評価の試み
― 日本とオーストラリアの各１０地点を対象として ―

Accuracy evaluation for GCOM-C ETindex estimation algorithm in forest areas – at 10-each sites in Japan and Australia

○梅野大樹[1]・多炭雅博[1]・篠原慶規[1]
Hiroki Umeno, Masahiro Tasumi, Yoshinori Shinohara

Abstract **:** In this study, the estimation performance of GCOM-C ETindex estimation algorithm was evaluated by comparing estimated annual evapotranspiration with observation values from literatures, at 10-each forest site in Japan and Australia. Estimation was made by applying the algorithm to MODIS thermal imagery for seven years from 2001 to 2007. There are two primary limitations on this research; one is the inconsistency in the target years between observation and estimation, and the other is the expected mixel problem by the coarse resolution of the satellite image pixel. However, the result of the comparison is valuable, because it provides initial idea regarding the estimation accuracy of the algorithm in annual time scale, in forest areas. As a result, clear positive relationships between observed and estimated evapotranspiration were confirmed both in Japan and in Australia. Observed and estimated values were close in some points, while it was not close in some other points. In both region, root-mean-squared-error was about 20% of average evapotranspiration. Future studies include the detailed analyses of this results, and enhancement of similar comparison to the different regions in the world.
Keywords **:** *GCOM-C, ETindex, evapotranspiration, forest*

1. はじめに

水資源のひっ迫している地域は現在世界中に多数存在する。また将来的には水需要のさらなる増加や、気候変動の影響による供給の不安定化が見込まれる。これらの水資源問題に対応するためには、データに基いた戦略的な水資源管理技術が必要である。地域の水資源の課題は流域単位での水収支に依存する部分が大きいので、広域を面的に観測することのできる衛星リモートセンシング技術の利用が有効である。水循環の主要プロセスの一つであり、土壌水分量や作物の生育にも大きく関係している蒸発散についても、SEBAL や METRIC などの衛星リモートセンシングモデルを使った推定が近年盛んにおこなわれている。

蒸発散推定における衛星リモートセンシング技術の利用は、流域単位のみならず全球規模でも有用である。しかし限られた面積の流域規模に比べて、膨大な衛星データ解析が必要な全球規模での蒸発散量推定では、推定アルゴリズムの自動化等の難しさがある。本研究では全球蒸発散推定アルゴリズムとして開発された GCOM-C ET index アルゴリズム (Tasumi et al. 2016a)について、推定精度情報の不足している森林域において、文献値を使った蒸発散量推定の精度検証に取り組んだ。

[1] 宮崎大学農学部
（〒889-2155 宮崎県宮崎市学園木花台1-1）
（連絡先 Tel；0985-58-7991、
E-mail；tasumi@cc.miyazaki-u.ac.jp ）

2. 研究方法

2-1. 森林蒸発散量検証用データの収集

Komatsu et al.(2012)は、膨大な文献調査を通して世界 829 か所の森林域における蒸発散量の実測あるいは推定データをまとめている。本研究ではこの論文に掲載された蒸発散量データ（文献値）の中から、日本とオーストラリアにおける各 10 地点を選定し、GCOM-C ET index アルゴリズムの推定精度検証用データとした。なお、Komatsu et al. (2012) に付与されている蒸発散量データは正確な位置情報等が与えられていないため、このデータをそのまま本研究に使用することはできない。そこで本研究では Komatsu et al. (2012)に掲載されたデータの引用文献リストを手掛かりに、引用元文献から蒸発散量データを直接収集し、森林蒸発散量検証用データを再構築した。各 10 地点を選ぶ際には、以下の点に配慮した。

(1) 文献の入手が容易であること（例：宮崎大学図書館が購読契約している雑誌掲載の論文等）。
(2) 文献に、緯度・経度・流域面積その他の、観測地や観測データに関する情報が正確に記載されていること。
(3) 本研究で検証を試みる全球蒸発散量マップの空間分解能が 5km×5km であるため、文献に示された観測地の森林がこの空間分解能に概ね見合う広域性を備えていること。また全球蒸発散量マップの比較対象とする「森林」ピクセル

の一部に海面が混入するのを防ぐため、海岸から概ね 5km 未満の沿岸部に位置する森林は検証用データとして採用しない。

なお本研究では、文献記載の観測地点の状況を個別に Google Earth で目視確認することにより、対象地が現在（あるいは近年）でも存在しているかどうか、また文献記載の位置情報が正確であるかどうかを確認した。位置が不明確あるいは不正確であった場合には、文献記載の住所や標高を手掛かりに実際の調査地を個別に推定した。この位置確認の際、同時に上記(3)で言及した広域性についても目視確認を行い、広域性がある程度担保できる地点のみを選定した。検証用蒸発散量データとして選定した観測地点の詳細を以下に示す。

2-1-1. 日本における観測地点

(A) 宝川本流

宝川試験地(北緯 36 度 51 分 東経 139 度 01 分)群馬県の北部、利根川の源流域にある。奥利根根水源地域のブナを主とする原生林の開発にあたり、森林の伐採と流出量の関係を明らかにすることを目的に調査が始まった。

調査期間は 1938-1947 年、流域面積は 19.06 ha、標高は 805-1945 m（平均 1391 m）。森林の種類は天然混交林である。また、森林総合研究所の森林理水試験地データベースによると、地質は花崗岩、凝灰岩、閃緑岩であり、土壌の種類は褐色森林土壌またはポドゾル、天然林における植生の優占は、ブナ、ミズナラ、イタヤカエデ、ホオノキ、ヒバ、ヒメコマツである。一方、人工林での優占はカラマツとスギが占めている。流域面積自体は本研究で使用する推定蒸発散量データの空間分解能（5km×5km）に対して極小であるものの、Google Earth の目視確認によると周囲は広範囲にわたり類似の森林に覆われている。

(B) 筑波試験地

筑波森林水文試験地（北緯 36 度 10 分 21 秒 東経 140 度 08 分 27 秒）。論文記載の座標とは異なる場所に林地が存在しており、Google Earth を用いて標高や住所を元に観測地点の位置を決定した。対象期間は 1979-1987 年、流域面積は 3.786 ha、標高は 290-390 m。森林の種類は針葉樹人工林である。また、筑波森林水文試験地観測報告によると、平均傾斜は 25 度、地質は、筑波変成岩類の黒雲母片麻岩が大部分を占めており、一部花崗岩の貫入がみられる。土壌は褐色森林土壌であり対象地の尾根側では Bb 型の土壌、谷側では Bd 型の土壌が卓越しており、谷川の中腹では Bc 型の土壌が発達している。この地点も流域面積自体は本研究で使用する推定蒸発散量データの空間分解能（5km×5km）に対して極小であるものの、Google Earth の目視確認によると周囲はおよそ 4km×4km の範囲にわたり類似の森林に覆われており、一部 5km×5km ピクセル内に農地等周辺土地被覆の混入が見込まれるものの、検証用データとして利用可能であると判断した。

(C) その他 7 地点について

その他 7 地点の詳細情報は割愛するが、7 地点を含む全 10 地点の場所と位置情報、引用元文献を表 1 にまとめる。

表 1. 日本の観測地点と引用元文献

観測場所	引用
去川Ⅱ (N31 51　E131 13)	Komatsu et al.(2008)
鹿北Ⅲ（N33 08　E130 42)	Komatsu et al.(2008)
宝川本流（N36 51　E139 01)	Komatsu et al.(2008)
筑波（N36 10　E148 08　)	Komatsu et al.(2008)
ぬたの谷（N34 27　E136 14　)	Komatsu et al.(2008)
定山渓 1（N42 58　E141 10)	Komatsu et al.(2008)
常陸太田（N36 54　140 35)	Komatsu et al.(2008)
白川谷　(N33 52　E133 54)	Yao et al. (1996)
南明治（N26 34　E128 01)	Komatsu et al.(2008)
辺土名（N26 44　E128 13)	Komatsu et al.(2008)

2-1-2. オーストラリアにおける観測地点

(A) Oliver Creek

オーストラリア北東部の熱帯地域に位置している（南緯 16 度 08 分 03 秒　東経 145 度 26 分 04 秒）。対象期間は 2002 年 8 月 17 日-2003 年 12 月 31 日。流域面積は 64ha。標高 30 m。傾斜は 4%、年平均気温は 23.5℃、年平均湿度は 93.0%である。

(B) Upper Baron

オーストラリア北東部の熱帯地域に位置している（南緯 17 度 21 分 01 秒　東経 145 度 29 分 07 秒）。対象期間は 2003 年 9 月 13 日-2005 年 6 月 30 日。流域面積は 69 ha。標高は 1050 m。た、傾斜は 20%、年均気温は 18.3℃、年均湿度は 93.9%である。

(C) その他 7 地点について

その他 7 地点の詳細情報は割愛するが、7 地点を含む全 10 地点の場所と位置情報、引用元文献を表 2 にまとめる。

表 2. オーストラリアの観測地点と引用元文献

観測場所と出典
Banbinda Creek at the Boulders (S17 20　E145 52) Chiew and McMahon (1994)
Canning River at Glen Eagle (調査地 1 S32 51 E116 15　調査地 2 S33 00 E116 07) Chiew and McMahon (1994)
Howard River (調査地 A S12 27 E131 03 調査地 E S12 30 E131 07) McJannet et al. (2007)
Mount Lewis1 (S16 31 07　E145 16 07) McJannet et al. (2007)
Oliver Creek (S16 08 03　E145 26 04) McJannet et al. (2007)
Upper Baron (S17 21 01　E145 29 07) McJannet et al. (2007)
Bellender Ker (S17 16 00　E145 16 07) McJannet et al. (2007)
March Road (S34 29 23　E116 19 44) Bari et al. (1996)
April Road South (S34 29 50　E116 21 20) Bari et al. (1996)
Lewin North (S34 10 35　E115 50 07) Bari et al. (2005)

2-2. 全球蒸発散量マップ

本研究にて精度検証に取り組む全球蒸発散量マップは、2001 年-2007 年までの 7 年間の MODIS 熱赤外観測画像を使用し、GCOM-C ETindex アルゴリズム（Tasumi et al., 2016a）により推定したものである。本研究に使用した全球蒸発散量マップについて、その入力データや推定手順を含む概要は Tasumi et al. (2016b)にまとめられている。ここではその概要のみ記載する。GCOM-C ETindex アルゴリズムは、衛星の熱赤外観測画像と全球風速データから蒸発散量の指標である ETindex を推定する。また全球気象データ（日射量・温湿度・風速）の利用により、実蒸発散量が推定できる。ETindex 推定には以下のような正規化式を使用する。

$$ET_{index} = C_{adj} \times \frac{T_s(\mathrm{dry}) - T_s(\mathrm{act})}{T_s(\mathrm{dry}) - T_s(\mathrm{wet})} \qquad (1)$$

ここで Ts(dry)，Ts(wet)はそれぞれ計算により求めた乾燥状態と湿潤状態の地表面温度、Ts(act)は衛星観測による実地表面温度、C_{adj} は係数。

気象データから基準蒸発散量を求めることで、ETindex は以下のように実蒸発散量に変換できる。

$$ET = ETindex \times ETo \qquad (2)$$

ここで ETo は FAO のマニュアル（Allen et al., 1998）により定義される基準蒸発散量。

MODIS の熱赤外観測の空間分解能は 1km なので、理論的には 1km の空間分解能での蒸発散推定が可能であるが、今回は解析環境の制約上、1.875°（中緯度地域で概ね 5km×5km）の空間分解能で計算した。本研究で使用した蒸発散量マップを図 1 に示す。

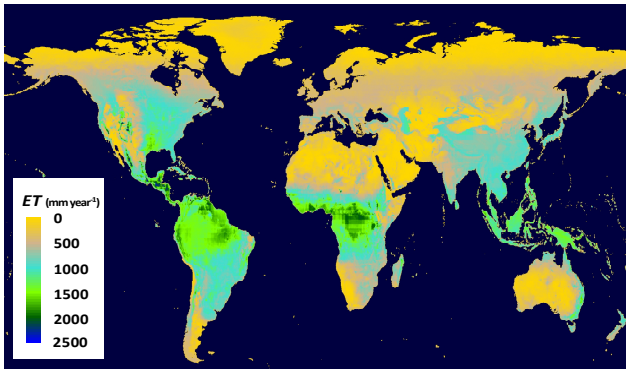

図 1. 全球実蒸発散量マップ（2001 年の例）

2-3. 精度評価方法

全球蒸発散量の推定精度を評価する試みとして、2-1 節で述べた検証用蒸発散量データ（実測値）と、2-2 節で述べた全球蒸発散量マップにおける当該ピクセルの蒸発散推定値とを比較した。検証用蒸発散量データはそれぞれの観測期間における年平均値、全球蒸発散量マップの推定値は 2001 年-2007 年の年平均値を使用した。

この比較方法には以下の 2 つの問題点がある。①比較する 2 つのデータの間の年（あるいは期間）が異なる。②全球蒸発散量マップの空間分解能が検証用データの観測対象区域に比べて粗いため観測対象外区域の情報が一定割合混入する。これら 2 点の制限はあるものの、このようなアプローチは衛星プロダクトの大まかな精度情報を把握する上では有用である。評価指標としては線形モデルの各種統計要素（傾き・切片・R^2）と RMSE を使用した。

3. 結果と考察

3-1. 日本における蒸発散量の推定精度

2-1-1 節で説明した 10 地点における、ET actual、ET estimate、ET difference の数値を表 3 にまとめる。ここで ET difference は ET actual と ET estimate の差である。2-1-1 節にて観測地点情報を概説した 2 地点に注目すると、宝川本流では、ET estimate が ET actual を上回っていることが分かる。一方、筑波試験地では ET estimate が ET actual を下回っている。10 地点のうち ET estimate が ET actual を上回った地点が 4 地点、下回った地点が 6 地点あった。

表 3. 日本国内 10 地点における森林蒸発散量の実測値と推定値の比較

観測地点	ET actual	ET estimate	Difference
去川 Ⅱ	931	1078	-147
鹿北 Ⅲ	874	935	-61
宝川本流	736	556	180
筑波	686	748	-62
ぬたの谷	979	807	172
定山渓 1	601	408	193
常陸太田	760	546	214
白川谷	964	517	447
南明治	1078	1094	-16
辺土名	1153	1114	39
平均	876	780	96

表 3 に示した 10 地点の実測および推定蒸発散量の分布を図 3 に示す。回帰直線の傾きは 1.12 で R^2 は 0.56 であった。また、RMSE の値は 194mm であった。この図から ET actual が ET estimate との関係性には正の相関があることがわかった。

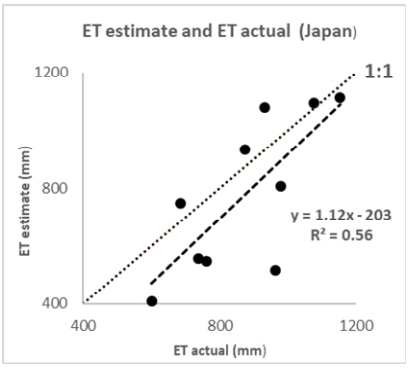

図 3. ET estimate と ET actual の線形グラフ（日本）

3-2. オーストラリアにおける蒸発散量の推定精度

2-1-2 節で説明した 10 地点における、ET actual、ET estimate、ET difference の数値を表 4 にまとめる。ここで ET difference は ET actual と ET estimate の差である。2-1-2 節にて観測地点情報を概説した 2 地点に注目すると、Oliver Creak、Upper Baron ともに、ET estimate が ET actual を上回っていた。ただし、ET estimate が ET actual を下回っていた地点も存在した。10 地点のうち ET estimate が ET actual を上回った地点が 5 地点、下回った地点が 5 地点あった。

表 4. オーストラリアの 10 地点における森林蒸発散量の実測値と推定値の比較

観測地点	ET actual	ET estimate	Difference
Banbinda Creek at the Boulders	1307	700	607
Canning River at Glen Eagle	724	780	-56
Howard River	1062	1110	-48
Mount Lewis1	1596	1533	63
Oliver Creek	1228	1298	-70
Upper Baron	1327	1518	-191
Bellender Ker	1336	971	365
March Road	844	843	1
April Road South	841	795	46
Lewin North	900	911	-11
平均	1116	1046	70

表 4 に示した 10 地点の実測および推定蒸発散量の分布を図 4 に示す。回帰直線の傾きは 0.74 で R^2 は 0.46 であった。また RMSE の値は 235mm であった。この図から ET actual が ET estimate との関係性には正の相関があることがわかった。オーストラリアの検証地点 10 地点については、Banbinda Creek at the Boulders と Bellender Ker の 2 地点が 1:1 ラインから大きく外れており、その他 8 地点については 1:1 ラインの近辺に分布するという結果になった。この、他の 8 地点と違った傾向を示した 2 地点について、実測側あるいは推定側に何らかの原因があるのかどうか、今後詳しく調査する必要がある。

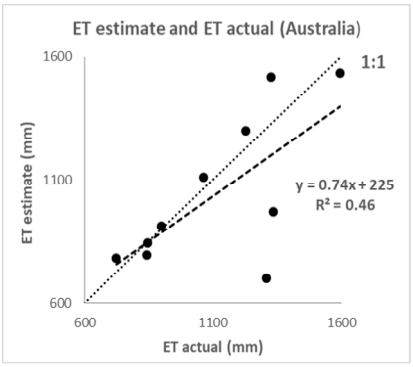

図 4. ET estimate と ET actual の線形グラフ（Australia）

4. おわりに

本研究では GCOM-C ETindex アルゴリズムによる推定蒸発散量の精度比較を日本 10 地点、オーストラリア 10 地点の計 20 地点で行った。実測データと推定データの対象年度が合致していない等、推定精度検討上の制約はあったものの、日本、オーストラリアともに実測値と推定値の間には強い正の相関が認められた。またいずれの地域でも RMSE が平均実蒸発散量の 20%程度の値を示した。実測値と推定値が概ね 1:1 ラインに乗っているデータと、大きく外れているデータがあるので、今後データをより詳細に検討して、実測値と推定値の乖離が大きい地点に何らかの原因があるのかどうか調査したうえで、地域間に特性の差があるかどうか検討を進めたい。

また、全球蒸発散量マップは全球を対象としているので、多くの地域について精度評価を行うことが大切である。今後、北メリカ、南アメリカや東南アジアなど、今回調査した地域以外の地域まで調査対象を広げたい。今後さらに精度評価を進めることにより、GCOM-C 蒸発散指数(ET index)プロダクトのアルゴリズムの改善に役立てていきたい。

謝辞

本研究は JAXA 地球環境変動観測ミッション(GCOM)共同研究「GCOM 陸圏プロダクトとしての蒸発散指数（作物係数）の開発」による研究費助成を受けて行われた。

引用文献

1) Allen, R. G., Pereira, L. S., Raes, D., and Smith, M., 1998: Crop Evapotranspiration—Guidelines for computing crop water requirements, FAO Irrigation and Drainage Paper 56. FAO, Rome, Italy. 330pp.
2) Bari, M.A., Smettem, K.R.J., and Sivapalan, M. 2005. “Understanding changes in annual runoff following land use changes: a systematic data-based approach.” Hydrological Processes. 19:2463-2479.
3) Bari, M.A., Smith, N., Ruprecht, J.K., and Boyd, B.W. 1996. “Changes in streamflow components following logging and regeneration in the southern forest of Western Australia.” Hydrological Processes. 10:447-461.
4) Chiew, F., and Mcmahon, T. 1994. “Application of the daily rainfall-runoff model MODHYDROLOG to 28 Australian catchments.” Journal of Hydrology. 153:383-416.
5) Cook, P.G., Hatton, T.J., Pidsley, D., Herczeg, A.L., Held, A., O’Grady, A., and Eamus, D. 1998. “Water balance of a tropical woodland ecosystem, Northern Australia: a combination of micro-meteorological, soil physical and groundwater chemical approaches.” Journal of Hydrology. 210:161-177.
6) Komatsu, H., Cho, J., Matsumoto, K., and Otsuki, K. 2012. “Simple modeling of the global variation in annual forest evapotranspiration.” Journal of Hydrology. 420-421:380-390.
7) Komatsu, H., Maita, E., and Otsuki, K. 2008. “A model to estimate annual forest evapotranspiration in Japan from mean annual temperature.” Journal of Hydrology.348:330-340.
8) McJannet, D., Wallace, J., Fitch, P., Disher, M., and Reddell, P. 2007. “Water balance of tropical rainforest canopies in north Queensland, Australia.” Hydrological Processes. 21:3473-3484.
9) Tasumi, M., Kimura, R., Allen, R.G., Moriyama, M., and Trezza, R. 2016a. “Development of the GCOM-C global ET index estimation algorithm.” Journal of Agricultural Meteorology. 72:85-94.
10) Tasumi, M., Moriyama, M., Hirakawa, K., and Fujii, A. 2016b. “Evaluation of the GCOM-C global ET index estimation algorithm.” Journal of Agricultural Meteorology. 72:151-158.
11) Yao, H., Hashino, M., and Yoshida, H. 1996. “Modeling energy and water cycle in a forested headwater basin.” Journal of Hydrology. 174:221-234.

衛星から推定された地表面温度検証候補地の選定
The flux site selection scheme for the satellite derived land surface temperature validation

○穐吉寿明、岡部嘉輝、森山雅雄[1]
Toshiaki AKIYOSHI, Yoshiki OKABE, Masao MORIYAMA

1. はじめに

2017 年 12 月 22 日、種子島宇宙センタから地球観測衛星「しきさい」が打ち上げられた、現在「しきさい」は順調に初期チェックを継続しており、2018 年 4 月には定常観測が開始され、12 月にはデータの一般公開がなされる予定である。長崎大学森山研究室では、「しきさい」に搭載された地球観測センサ SGLI (Second generation GLobal Imager)で得られた熱赤外データから地表面温度を推定するアルゴリズムを開発している。アルゴリズム開発者は、その検証まで責任を持つ必要があるため、本研究室では、衛星から推定された地表面温度の定常的な検証手法の開発も実施している。本研究は、エネルギおよび物質輸送を常時計測しているフラックスサイトでの長波放射観測データの地表面温度検証への利用可能性を把握するため、時空間的に地表面温度が一様なサイトの選定手法について説明するものである。

2. フラックスサイトでの長波放射観測

フラックスサイトとは、タワーに各種計測器を設置し、地表面でのエネルギ、物質収支を定常的に計測している観測点であり、北米では Ameriflux、アジアでは Asiaflux といった団体が観測データの管理、配布を行っている。各フラックスサイトでは、地表が吸収する放射エネルギとして地表での放射収支を計測している。放射収支とは、地表面での下向き短波および長波放射から、上向き短波および長波放射を減じたものである。放射収支を観測するひとつの手段として、上向きおよび下向きの短波および長波放射を個別に計測する四成分放射計を用いることがある。図 1 に米国コロラド州ボールダー西部のフラックスサイトのタワーと、フラックスサイトでの放射観測の概念図を示す。

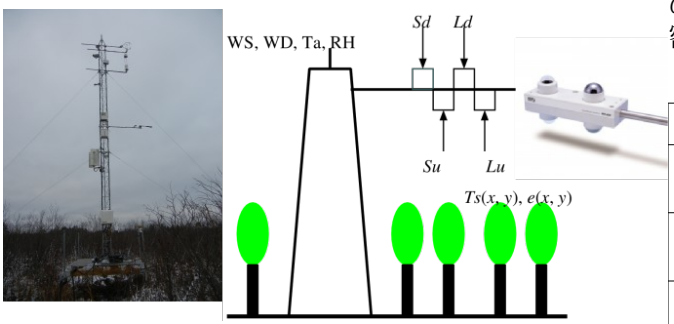

図 1 コロラド州ボールダーのフラックスサイト(左)とフラックスサイトでの放射観測概念図(右)

3. 長波放射観測値からの地表面温度推定

四成分放射計で計測された上向きおよび下向き長波放射照度をそれぞれ、*Lu*, *Ld* とするとそれらの関係は、地表面温度を *Ts*、地表面の広帯域射出率を *e* として式(1)で表される。

$$Lu = e\sigma Ts^4 + (1-e)Ld \qquad (1)$$

ここで、σ は、ステファン-ボルツマン係数であり、値は 5.67×10^{-8} [W m^{-2} K^{-4}]である。広帯域射出率を決定し、長波放射観測値を基に式(1)を解くことで地表面温度が得られる。

4. 地表面温度検証サイトに求められる性質

衛星から推定された物理量は、その一画素に渡る面平均値であるため、理想的には一画素内の複数点での地上観測が必要となる。しかし、そのような地上観測を定常的に実施するのは困難であるため、地表面の物理量が空間的に一様な場所での点計測値を検証に用いる必要がある。これに加えて地表面温度の場合は、風、日射など環境要因の変動に対して地表面温度が変化しにくいこと、および広帯域射出率が高く、時間的に変化しにくいことが必要となる。これらの性質を満たす土地被覆として、密な森林、特に年間通して検証を行うとすれば常緑樹林が地表面温度検証に適切であるといえる。

5. 地表面温度検証サイトの選定

上記の性質を満たすフラックスサイトを以下の手順で選定した。

i. Ameriflux の web から常緑樹林および落葉樹林を選択し、その緯度経度を把握する。
ii. Google earth でその位置を表示し、密な森林が広域にわたり一様なサイトを選択する。

上記の手順で選定したサイトを表 1 に示し、それらの Google earth からの画像を図 2 - 4 に示す。どれも密な森林がある程度広がっていることが把握できる。

表 1 選定された Ameriflux サイト

コード	緯経度	場所	森林種類
CA-Obs	53.99N, 105.12W	カナダ、サスカチュワン	常緑針葉
US-MMS	39.32N, 86.41W	米国、インディアナ州	落葉広葉
US-WRC	45.82N, 121.95W	米国、ワシントン州	常緑針葉

1　長崎大学工学部　〒852-8521 長崎市文教町 1-14
matsu@cis.nagasaki-u.ac.jp

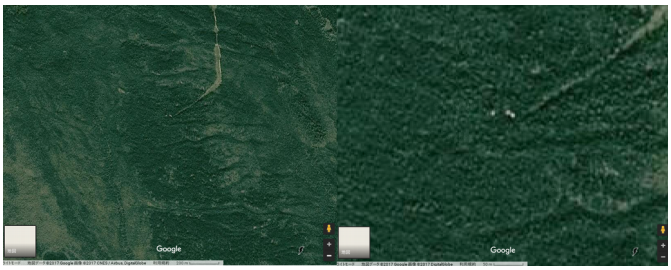

図 2 CA-Obs の google earth 画像(左: 上下 1km、右上下 100m)

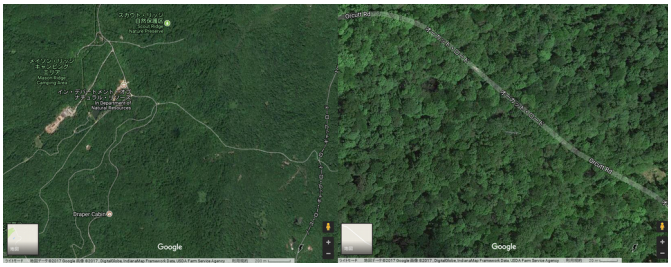

図 3 US-MMS の google earth 画像(左: 上下 1km、右: 上下 100m)

図 4 US-WRC の google earth 画像 (左: 上下 1km, 右: 上下 100m)

6. ASTER 輝度温度データによる温度の空間変動把握

google map の画像だけでは、温度の一様性が把握できないため、当該領域の空間分解能 90[m]の ASTER 輝度温度(見かけの温度)データを 250[m](SGLI の空間分解能)および 1[km](MODIS の空間分解能)で統計解析を行った。観測点周辺に直径 250[m]、1[km]のバッファを生成し、バンド 13 の輝度温度標準偏差を計算した。結果を図 5 – 7 に示す。図中赤は 250m、緑は 1km バッファの計算結果である。

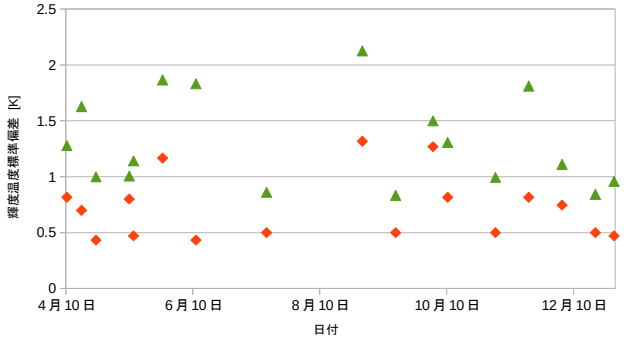

図 5 CA-Obs ASTER バンド 13 の輝度温度標準偏差 [K] (2006 年)

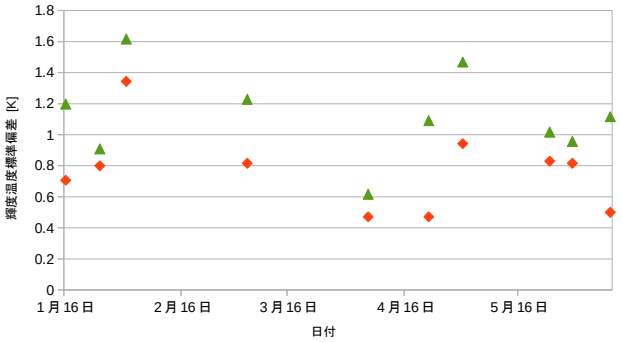

図 6 US-MMS ASTER バンド 13 の輝度温度標準偏差[K] (2006 年)

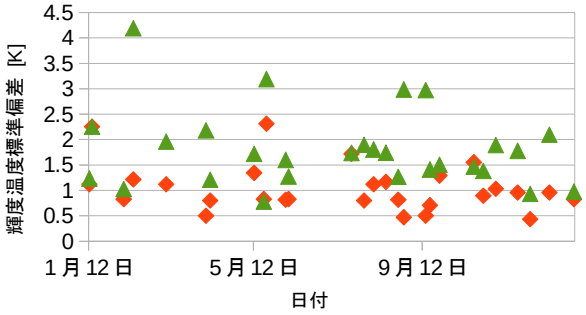

図 7 US-Wrc ASTER バンド 13 輝度温度標準偏差 [K] (2014 年)

輝度温度標準偏差は、その時期の SGLI または MODIS 一画素内の温度変動状況を反映していると考えられるため、ここに挙げた 3 点は SGLI の地表面温度検証に利用可能であることが示された。

7. 結論

フラックスサイトの長波放射観測データを用いた地表面温度プロダクト検証手順は以下のようになる。

I. 衛星観測時刻でのフラックスサイトでの長波放射観測データを収集し、式(1)から地表面温度を推定する。
II. 観測と近い時期の高空間分解能熱赤外データ(ASTER など)を収集し、観測点まわりの一画素分の領域の輝度温度標準偏差を計算し、それが十分小さければ、長波放射観測データからの地表面温度と衛星からの地表面温度を比較する。
III. 高空間分解能熱赤外データの輝度温度標準偏差を s、SGLI 一画素分の高空間分解能データの画素数を n とすると、区間推定理論より、信頼区間幅 δT は、式(2)で計算できるため、II の地表面温度と一緒に信頼区間幅も検証に用いる。

$$\delta T = \alpha \frac{s}{\sqrt{n}} \qquad (2)$$